# External and Internal Air Loads on Sounding Rockets

RALPH J. MURACA*
*NASA Langley Research Center, Hampton, Va.*

**This paper discusses two important forms of loading experienced by sounding rockets: the running loads due to distributed aerodynamics, and loads due to aerodynamically induced pressure differentials across the skin and across internal bulkheads. An empirical method, based upon experimental data, for the rapid and accurate determination of distributed aerodynamic loads on arbitrary bodies of revolution is outlined, and comparisons of typical results with wind-tunnel data are presented. In addition, the equations describing the venting of an "$n$" volume system have been derived and a comparison of experimental with analytical results for a four-volume system subjected to a typical launch pressure profile are included.**

## Nomenclature

| | | |
|---|---|---|
| $A$, $c$ | = | orifice area and discharge coefficient, respectively |
| $C_p$ | = | pressure coefficient |
| $C_{N\alpha}$ | = | normal force coefficient slope = $F_N/qS\alpha$ |
| $D$, $D_0$ | = | local body diameter and reference diameter, respectively |
| $f_a$ | = | fineness ratio = $l/D_0$ |
| $l$ | = | component length |
| $M$ | = | Mach number or total mass |
| $m$ | = | mass flow rate through an orifice |
| $p$ | = | pressure, psia |
| $q_\infty$ | = | freestream dynamic pressure, lb/in.$^2$ |
| $S_r$ | = | reference area |
| $S(dC_{N\alpha}/dx)$ | = | distributed normal force coefficient slope, in./rad |
| $t$ | = | time, sec |
| $V$ | = | volume |
| $w$ | = | running load, lb/in. |
| $\alpha$ | = | local angle of attack, rad or deg |
| $\gamma$ | = | ratio of specific heats |
| $\lambda$ | = | loading function = $(1/D)\ S(dC_{N\alpha}/dx)$ |
| $\rho$ | = | density, lb-sec$^2$/in.$^4$ |
| $\theta_n$, $\theta_f$ | = | cone half-angle and frustum angle, respectively |
| $\phi$ | = | polar coordinate |

***Subscripts***

| | | |
|---|---|---|
| $r$ | = | $r$th chamber quantity |
| $0$, $a$, $e$ | = | initial, reference, and external conditions, respectively |
| $n$ | = | total number of chambers |

## External Loads

THE inclusion of body flexibility in dynamic loads and stability analyses requires a detailed description of the normal force distribution on the body. Unlike the total aerodynamic coefficients, a standard nomenclature for distributed aerodynamic coefficients has not evolved. The notation used is $S(dC_{N\alpha}/dx)$, the product of the normal force coefficient derivative with respect to body length and an arbitrary reference area term. The distributed normal force coefficient for a typical launch configuration is shown in Fig. 1. This coefficient is converted into a running load by multiplying it by the appropriate value of local angle of attack and dynamic pressure. By integrating the running load curve over the length of the body and dividing by a reference area, a total normal force coefficient slope can be obtained.

Presented at the AIAA Sounding Rocket Vehicle Technology Specialist Conference, Williamsburg, Va., February 27–March 2, 1967 (no paper number; published in bound volume of papers of the meeting); submitted February 20, 1967; revision received May 4, 1967. [3.03, 11.16]

* Aerospace Technologist, Flight Vehicles and Systems Division.

An empirical method for rapidly determining distributed aerodynamic coefficients for arbitrary configurations has been developed.[1] It represents a compilation and correlation of available experimental results into a set of design curves that yield aerodynamic distributions for the various geometric components used in launch vehicle design. Force and pressure data are reduced to a nondimensional loading function $\lambda$ which is defined as the term $S(dC_{N\alpha}/dx)$ divided by the local body diameter (Fig. 2). The left-hand side of Fig. 2 shows $C_{N\alpha}$ vs frustum length for a configuration consisting of a fixed cone cylinder followed by a frustum. The frustum is divided into segments, and the curve is obtained stepwise by these segments until the desired frustum length is reached. To convert these data to $\lambda$ requires the differentiation of $C_{N\alpha}$ with respect to $D/D_0$, where $D$ is the frustum diameter at the point where the slope is being measured. The conversion of pressure test data to $\lambda$ is shown on the right-hand side of Fig. 2. The variation of the pressure coefficient $C_p$ with polar coordinate $\phi$ at station A for a frustum following a cone cylinder at $\alpha = 4°$ is displayed along with the relationship between $\lambda$ and $C_p$. The $\lambda$'s derived from force data in general do not reflect local perturbations; however, if the pressure sensors are properly located, a pressure model will reflect these perturbations. Figure 3 shows a typical set of $\lambda$ curves for frustums following cone cylinders. Such curves also have been published[1] for spherical segments, cones, cone frustums, cylinders, tangent ogives, and boattails.

The application of this method to a typical two-stage configuration requires little effort, and the computations can be done by hand; however, it has been programmed for machine computation. Sample results are compared with experimental data in Fig. 4 for three configurations. In Fig. 4a, agreement is good except in the region just behind the frustum at $M = 2.0$ and 2.36. Figure 4b is for a three-stage configuration similar to a Saturn upper stage. The experimental and empirical curves are quite similar except in the region of body slope discontinuities. This discrepancy is probably due to the fact that the $\lambda$'s used to generate these distribu-

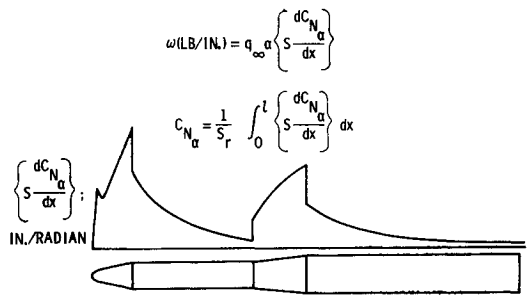


**Fig. 1 Typical normal force coefficient slope distribution.**

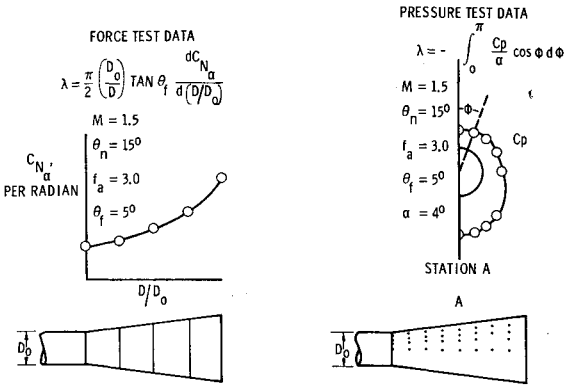


**Fig. 2 Reduction of force and pressure test data to loading functions.**

tions were obtained from wind-tunnel results that did not reflect significant flow separation. In general, this method would be expected to yield the best results at higher supersonic Mach numbers, since one of the primary assumptions is that the upstream λ's are independent of the downstream geometry. Figure 4c shows transonic data, and again the major discrepancies are due to flow separation effects in the vicinity of the cylinder frustum junction. For eight other configurations at four Mach numbers, the empirical total normal force coefficient slopes differed from wind-tunnel results by an average of 8.5%, and the centers of pressure differed by 0.33 diam.[2]

## Internal Loads

A second important class of aerodynamically-induced loads which must be considered in the design of a sounding rocket are those due to differential pressures occurring across internal bulkheads and across the vehicle outer surface. Improper design of a spacecraft launch-vehicle venting system can result in complete mission failure. Some means must be provided for venting internal cavities. Important factors affecting venting system performance are external vent locations and sizes, internal flow paths, and internal orifice sizes.

A typical $C_p$ distribution on a launch vehicle is shown in Fig. 5. Obviously, the pressure differential from a cavity across the outer skin could be altered by the placement of the external vents. However, in most instances other requirements exist which will affect the selection of the external vent location (e.g., prelaunch cooling requirements of various components, internal bulkhead load limitations, in-flight acoustical load levels, and prescribed thermal environments). It should be noted that the $C_p$ at a particular position on the body can depend strongly on Mach number, especially near surface slope discontinuities. The pressure differentials across the bulkhead separating compartments A and B in Fig. 5 have been calculated for forward and aft locations of the external vent. The pressure-time histories at each of these positions and the corresponding $\Delta P$'s across the bulkhead are shown in Fig. 6.

The maximum magnitude of $\Delta P_2$ (aft location of vent) is almost three times that of $\Delta P_1$ (forward location). Also note the dependence of $\Delta P$ upon the local slope of the external pressure curve; to keep the $\Delta P$'s low, external vents should be placed in regions where $P$ will not vary rapidly with time.

Most launch-vehicle internal cavities and vent paths can be considered as a series of chambers interconnected by orifices. To analyze such configurations, a set of descriptive equations utilizing isentropic relations has been formulated as an $n$-volume problem (see Appendix). Analytical results (solid curve) are compared with experimental data in Fig. 7. The vent model used was a four-volume configuration externally vented through volume 1. The calculated pressure

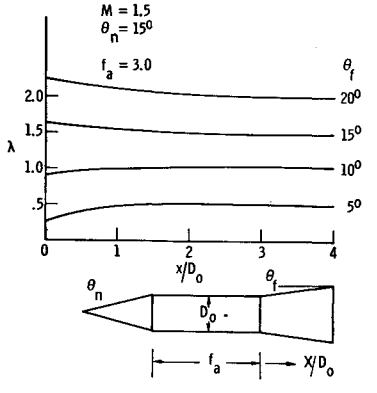


**Fig. 3 Loading functions for a frustum following a cone cylinder.**

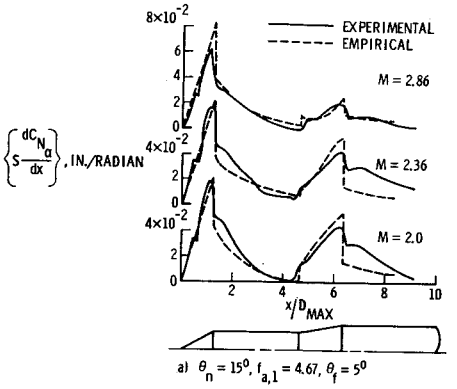


a)

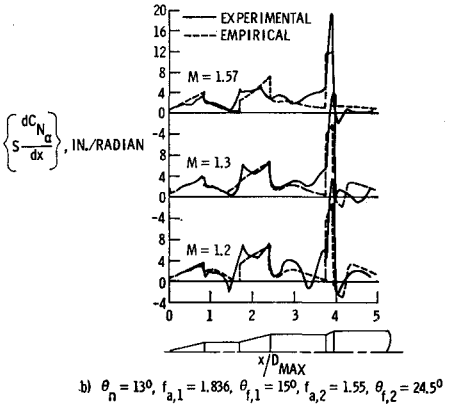


b)

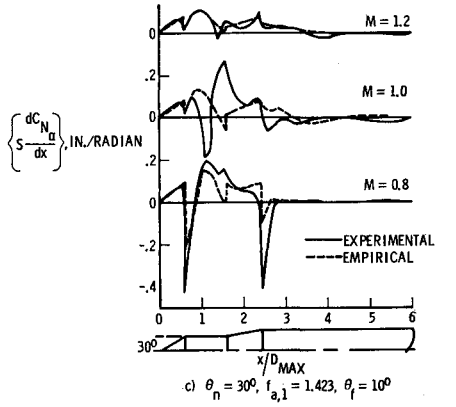


c)

**Fig. 4 Comparisons of experimental and empirical data.**

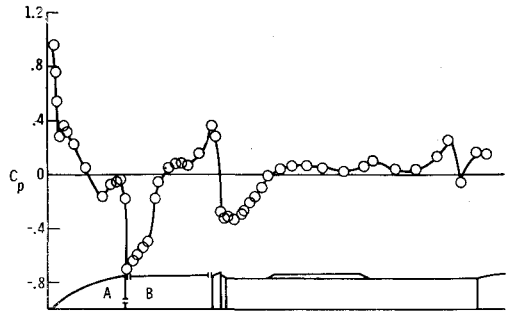


**Fig. 5 Pressure coefficient distribution on a typical spacecraft configuration.**

differentials shown in this figure were obtained using constant values of orifice discharge coefficients; however, Ref. 3 indicates that the discharge coefficient is a function of both Reynolds number and pressure ratio. Reynolds number during these tests ranged from about 50,000 to approximately 1000. Pressure ratios varied between 0.96 and 1.0. In addition, the shaded region shows the range of values of $\Delta P_4$ which were obtained from two different measurements: 1) by subtracting the measured $P_4$ from the measured $P_e$ and 2) by direct measurement of $P_4 - P_e$ using a differential pressure transducer.

In examining the trajectories of a variety of launch vehicles, it was found that the ambient pressure histories during ascent for certain groups of vehicles were quite similar when based upon an appropriate dimensionless time. Figure 8 shows $P/P_a$ vs $t/t_a$, where $P_a$ is sea-level ambient pressure and $t_a$ is the time required for a given vehicle to reach a reference altitude (120,000 ft) for two distinct categories of vehicles: fast-rising, smaller vehicles such as Nike-Apache, Raven, etc., and larger vehicles such as Scout, Atlas, etc. As will be shown, although these curves do not reflect the perturbations which a local pressure profile might exhibit, they can be very useful in determining preliminary data applicable to a given one-volume venting system.

If the $n$-dimensional equations derived in the Appendix are reduced to the case of a single volume, the following nondimensional first-order differential equations result:

$$\frac{d\bar{P}}{d\bar{t}} = -\beta\left\{\bar{P}^{(1+3\gamma)/2\gamma}\left[\left(\frac{\bar{P}_e}{\bar{P}}\right)^{2/\gamma} - \left(\frac{\bar{P}_e}{\bar{P}}\right)^{(\gamma+1)/\gamma}\right]\right\}^{1/2}$$

where

$$\beta = \left\{\frac{cAt_a}{V}\left(\frac{P_0}{\rho_0}\right)^{1/2}\left(\frac{2\gamma^3}{\gamma-1}\right)^{1/2}\right\}$$

where $A$ and $c$ are the area and coefficient of the orifice, respectively; $V$ is the chamber volume; $P_0$ and $\rho_0$ are the

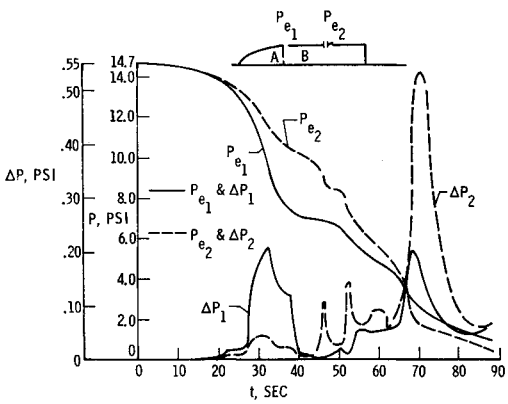


**Fig. 6 Variation in bulkhead pressure differential with external orifice location.**

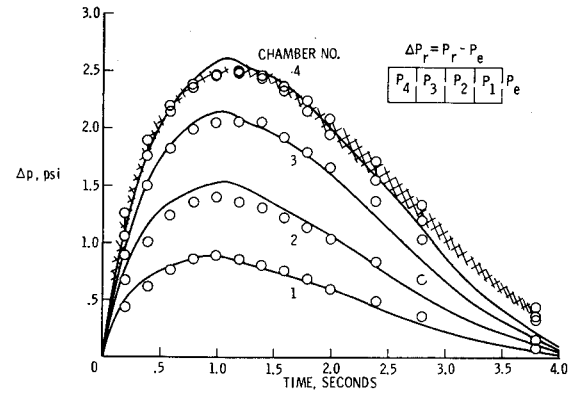


**Fig. 7 Comparison of calculated and measured pressure differentials.**

initial chamber pressure and mass density, respectively; $\bar{P} = P/P_0$; $\bar{P}_e = \bar{P}_e/P_0$; and $\bar{t} = t/t_a$. If an external pressure profile is used similar to either of the ascent pressure profiles shown in Fig. 8 and solutions are obtained for a wide variation in $\beta$, a set of design curves will result which can be used to estimate pressure differentials for a single-volume system. Typical curves for the smaller launch vehicles are shown in Fig. 9. Data for values of $\beta$ from 0.1 to 100 have been ob-

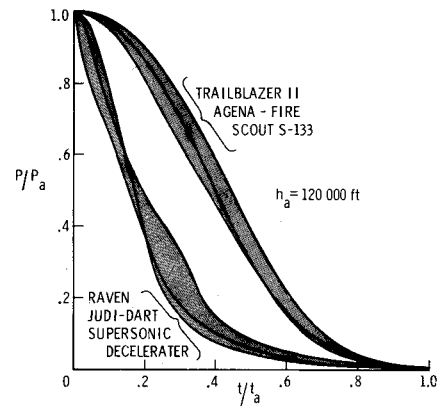


**Fig. 8 Typical ascent ambient pressure profiles.**

tained, and for specified values of $t_a$, $\gamma$, $c$, $P_0$, and $\rho_0$, these correspond to $A/V$ ratios of from $0.0918 \times 10^{-1}$ to $91.8 \times 10^{-6}$. Note that the time at which the peak pressure differential occurs increases as $\beta$ decreases. Since $P_e$ will, in general, differ from the ambient pressure, these data should only be used to yield estimated internal pressure profiles. A venting analysis of each specific configuration should be performed in most instances.

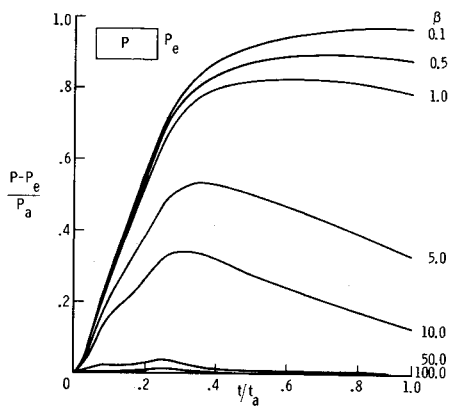


**Fig. 9 Effect of $\beta$ variation for a single-volume configuration.**

## Summary

In summary, a rapid and accurate empirical method for the determination of the distributed aerodynamic characteristics of arbitrary bodies of revolution has been outlined, and its accuracy has been illustrated by comparisons with wind-tunnel force and pressure data. The importance of panel loads due to transient pressure differentials has been discussed, and a mathematical solution for the transient pressure differentials in an $n$-volume, series-connected system vented to an arbitrary, time-varying pressure is appended. A set of design curves has been presented which can be used to estimate internal pressure time histories during the ascent phase of flight for sounding rockets having vented single volumes.


## Appendix

To predict the static panel loading on the surface of a launch configuration and the loading due to pressure differentials across internal bulkheads or diaphragms, one must determine the internal pressure time histories of the appropriate number of chambers connected in series to an external pressure source. In the following method the fluid is assumed to be perfect, the flow is assumed to be nonviscous and nonconducting, all processes are assumed to occur isentropically, and the fluid in each chamber is assumed to be homogeneous. For the $r$th chamber connected to a series of other chambers through a set of orifices, a mass balance can be written as follows. The total mass of fluid in it at any time is $M_r = \rho_r V_r$. Differentiating with respect to time yields $\dot{M}_r = \dot{\rho}_r V_r$, which must equal the rate at which mass flows across the chamber boundaries:

$$\dot{M}_r \equiv \dot{\rho}_r V_r = m_{r+1} - m_r \tag{A1}$$

where the signs are consistent with the assumption (but not the constraint) that $P_{r-1} < P_r < P_{r+1}$. The mass flow leaving the $r$th chamber through the $r$th orifice is

$$m_r = cA_r \left\{ \frac{2\gamma}{\gamma - 1} \rho_r P_r \left[ \left( \frac{P_{r-1}}{P_r} \right)^{2/\gamma} - \left( \frac{P_{r-1}}{P_r} \right)^{(\gamma+1)/\gamma} \right] \right\}^{1/2} \tag{A2}$$

and $m_{r+1}$ is given by the same equation, raising all subscripts by 1. If the processes are assumed to occur isentropically,

$$\rho = \rho_a \left( \frac{P}{P_a} \right)^{1/\gamma} \qquad \dot{\rho} = \rho_a \frac{P^{(1-\gamma)/\gamma} \dot{P}}{\gamma P_a{}^{1/\gamma}} \tag{A3}$$

where the subscript $a$ denotes some reference condition. Then

$$m_r = cA_r \left\{ \frac{2\gamma}{\gamma - 1} \frac{\rho_{r_a} P_r{}^{(\gamma+1)/\gamma}}{P_{r_a}{}^{1/\gamma}} \times \left[ \left( \frac{P_{r-1}}{P_r} \right)^{2/\gamma} - \left( \frac{P_{r-1}}{P_r} \right)^{(\gamma+1)/\gamma} \right] \right\}^{1/2} \tag{A4}$$

and a similar relation applies for $m_{r+1}$. From Eqs. (A1) and (A3) we obtain

$$\dot{P}_r = \gamma P_{r_a}{}^{1/\gamma} P_r{}^{(\gamma-1)/\gamma} (m_{r+1} - m_r)/\rho_{r_a} V_r \tag{A5}$$

These equations for $m_r$, $m_{r+1}$, and $\dot{P}_r$ form a set of $n - 2$ nonlinear, first-order differential equations in the dependent variable $P_r$, ($r = 2, 3, \ldots, n - 1$). For the first and last chamber, these equations must be altered slightly. For $r = 1$, Eq. (A4) becomes

$$m_1 = cA_1 \left\{ \frac{2\gamma}{\gamma - 1} \frac{\rho_{1_a}}{(P_{1_a})^{1/\gamma}} (P_1)^{(1+\gamma)/\gamma} \times \left[ \left( \frac{P_e}{P_1} \right)^{2/\gamma} - \left( \frac{P_e}{P_1} \right)^{(\gamma+1)/\gamma} \right] \right\}^{1/2} \tag{A6}$$

where $P_e$ can be an arbitrary function of time. For the last chamber, $r = n$, and $m_{n+1} = 0$, since $A_{n+1} = 0$. The foregoing set of $n$ nonlinear first-order differential equations can be programmed for solution on automatic computers.

## References


[1] Muraca, R. J., "An empirical method for determining static distributed aerodynamic loads on axisymmetric multistage launch vehicles," NASA TN D-3283 (March 1966).

[2] Samuels, R. D. and Blackwell, J. A., Jr., "Effects of configuration geometry on the supersonic aerodynamic characteristics of a simulated launch vehicle," NASA TN D-3755 (January 1967).

[3] Nelson, W. J. and Dewey, P. E., "A transonic investigation of the aerodynamic characteristics of plate- and bell-type outlets for auxiliary air," NACA RM L52H20 (September 1952).